Geosynthetic Encased Column: comparison between numerical and experimental results

Nima Rostami Alkhorshid[1#] 🆔 , Gregório Luís Silva Araújo[2] 🆔 ,

Ennio Marques Palmeira[2] 🆔

Article

Abstract
The use of granular column is one of the ground improvement methods used for soft soils. This method improves the foundation soils mechanical properties by displacing the soft soil with the compacted granular columns. The columns have high permeability that can accelerate the excess pore water pressure produced in soft soils and increase the undrained shear strength. When it comes to very soft soils, the use of granular columns is not of interest since these soils present no significant confinement to the columns. Here comes the encased columns that receive the confinement from the encasement materials. In this study, the influence of the column installation method on the surrounding soil and the encasement effect on the granular column performance were investigated using numerical analyses and experimental tests. The results show that numerical simulations can reasonably predict the behavior of both the encased column and the surrounding soil.

1. Introduction

Construction on soft soils is one of the most significant challenges for geotechnical engineers. One of the solutions is the use of granular columns to improve the composite foundation soil overall shear strength. The performance of granular columns is highly dependent on the confinement provided by the surrounding soil. This technique is not recommended in very soft soils (S_u < 15 kPa), since these soils present low shear strength and high compressibility. In this context, the lack of confinement around the column can be overcome using geosynthetic encasement. In recent years, many projects used geosynthetic encased columns to stabilize the soft soil foundation (De Mello et al., 2008; Araujo et al., 2009; Gniel & Bouazza, 2009; Alexiew & Raithel, 2015; Xue et al., 2019; Chen et al., 2020). Encased granular columns act like semi-rigid piles that transfer the loads to the soil layers at specific depths capable of bearing them. Moreover, they function like vertical drains and provide radial drainage to the soft soils and accelerate the consolidation process. Besides providing lateral confinement to the column, geotextiles protect them from the clogging of the granular infill material (Castro & Sagaseta, 2011; Zhang et al., 2012; Pulko & Logar, 2017; Li et al., 2020; Chen et al., 2020).

The influence of encasement on the granular column performance was appraised in various experimental studies. In these studies, partial and full encasement of the granular columns were investigated. The results showed that the encasement could increase the bearing capacity and reduce the settlement of the column (Yoo & Lee, 2012; Ali et al., 2012; Xue et al., 2019; Alkhorshid, 2017; Zhang et al., 2020; Cengiz & Guler, 2020; Chen et al., 2020; Alkhorshid et al., 2020).

The Finite Element Method (FEM) is a powerful tool to investigate geotechnical problems and can be calibrated using laboratory and field data and, consequently, be utilized for large-scale projects (Alkhorshid, 2012; Keykhosropur et al., 2012; Castro & Sagaseta, 2013; Alkhorshid et al., 2014; Mohapatra et al., 2017; Nagula et al., 2018, Alkhorshid et al., 2021). Despite various studies that have been done to investigate encased granular columns, the current knowledge on their performance still needs improvement. In this study, the displacement installation method's effect on the surrounding soil and the encasement influence on the granular column behavior were evaluated using laboratory tests and numerical analyzes. Laboratory tests were analyzed using PLAXIS 3D and 2D to evaluate the numerical analysis capability in predicting soft soil and column behavior.

#Corresponding author. E-mail address: nimara@unifei.edu.br
[1]Universidade Federal de Itajubá, Institute of Integrated Engineering, Itabira, MG, Brasil.
[2]Universidade de Brasília, Department of Civil and Environmental Engineering, Brasília, DF, Brasil.

2. Model test

2.1 Test setup

The test tank, with dimensions 1.6 m × 1.6 m × 1.2 m (Figure 1), was covered internally by lubricated plastic sheets to make it impermeable before placing the soft soil inside the tank and reduce friction along the internal faces of the tank. A scale factor (λ = prototype diameter/model diameter) of 4 (Alkhorshid et al., 2019) was used to reach the desired soil undrained shear strength (S_u < 5 kPa), column diameter (d_c = 0.15 m) and geotextile tensile stiffness (J < 125 kN/m) for laboratory modeling. The soft soil was allowed to consolidate under self-weight before the column installation. Four piezometers were installed in the soft soil to monitor the effects of column installation on the soil pore water pressures during the tests, as shown in Figure 1.

2.2 Installation method

The displacement method was adopted to install the column. The encased column was prepared outside of the test tank using vibration to reach a target relative density of 85%. The column infill was placed and vibrated inside a closed-tip (by a non-woven geotextile) geotextile encasement in layers 20 cm thick. Then, the column was placed inside a PVC pipe closed at the tip. A wooden casing (Figure 2) was used to keep the column perpendicular to the tank base during installation. By driving the column inside the soft soil, the surrounding soil displaces laterally and influences the soil mechanical and physical properties.

2.3 Boundary conditions and numerical modeling

To simulate the model tests in PLAXIS 2D and 3D (Figure 3), roller and pinned supports were applied to the lateral and base boundaries, respectively. Thus, the soft soil was able to displace vertically at the tank sides, but horizontal and vertical displacements were restrained at the base. Undrained conditions were adopted for the lateral and base boundaries to avoid water flow, since the tank was internally covered with plastic sheets.

The Soft Soil model is an appropriate model for normally consolidated clay, which was the case in this study. The Mohr-Coulomb model was adopted to simulate sand, gravel and recycled construction and demolition waste (RCDW – composed of broken bricks, concrete, and gravel) used as column infill materials (Khabbazian et al., 2010; Keykhosropur et al., 2012; Alkhorshid, 2012; Almeida et al., 2013; Alkhorshid et al., 2014, 2018). The properties of materials used in the numerical simulations, obtained from laboratory tests and back analysis, are given in Table 1 (Alkhorshid, 2017; Alkhorshid et al., 2019). The model geotextile encasement with the desired diameter (d_c = 0.15 m) and tensile stiffness (J < 125 kN/m) was not commercially available. Therefore, three types of geotextile encasements, G1 (J = 120 kN/m), G2 (J = 107 kN/m) and G3 (J = 53.4 kN/m), were used in this study to account for the scale factor (λ). Seam was used along the column length, which made it an anisotropic material, with different tensile stiffness along vertical and circumferential directions. Consequently, the geotextile encasements were simulated using elastic material with two different values of tensile stiffness in these directions (Table 2). Interface elements were applied to simulate the interactions between
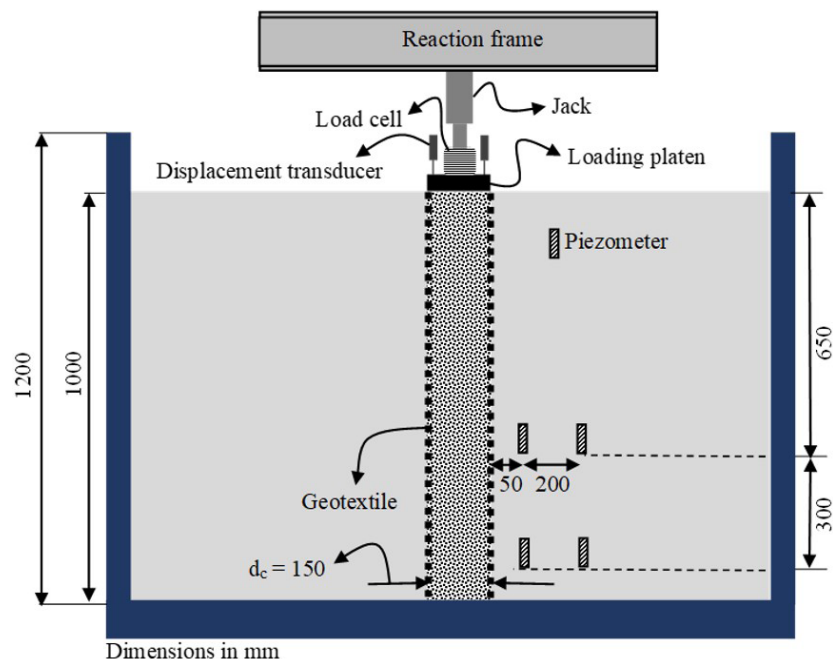

Figure 1. Schematic view of the equipment.

the geotextile encasement and the adjacent materials (soft soil and column infill), and the strength reduction factor (R_{int} – see Table 1) was assigned to specify these interactions.

An axisymmetric model (6-noded elements) in PLAXIS 2D was analyzed using consolidation analysis to evaluate the installation effects (excess pore water pressure, undrained shear strength and soil heave) on the surrounding soil. A cylindrical cavity with a radius of 0.02 m was applied to the soil to enable lateral prescribed displacement (equal to the column radius, 0.075 m). Actually, the column is driven into the soil, and during penetration the soil is displaced laterally. However, in this numerical analysis, the cavity approach (Castro & Karstunen, 2010) was required to apply lateral displacements. Results of laboratory column bearing capacity tests were back analyzed using PLAXIS 3D (Alkhorshid, 2017; Alkhorshid et al., 2019). Hence, the prescribed settlements and their corresponding loads were compared to the laboratory results.

3. Numerical and model tests results

3.1 Load-settlement curves

The results obtained from the laboratory tests (Figure 4a) show conventional (uncased) column inability to bear significant loads. The differences between the load capacities carried by the three different columns (sand, gravel, and RCDW) are negligible, which was predictable since these columns received no significant confinement from the surrounding soft soil. The numerical results are in satisfactory agreement with those from the tests. The numerical prediction for RCDW compared better with the test results.

Figures 4b and 4c show the importance of the geotextile encasement in improving the column bearing capacity and show that the numerical results compare well with those from the tests. Still, the numerical results obtained for G3 (Figure 4b) show some differences as the load increases, leading to an overestimation of 8.5% at the end of the test. Figure 4c shows that the numerical results for G2 do not perfectly fit those from the tests at the early stages of the test. Thus, the numerical predictions underestimated the load values by as much as 10% in these stages.

Figure 2. Installation of the column using a wooden casing.
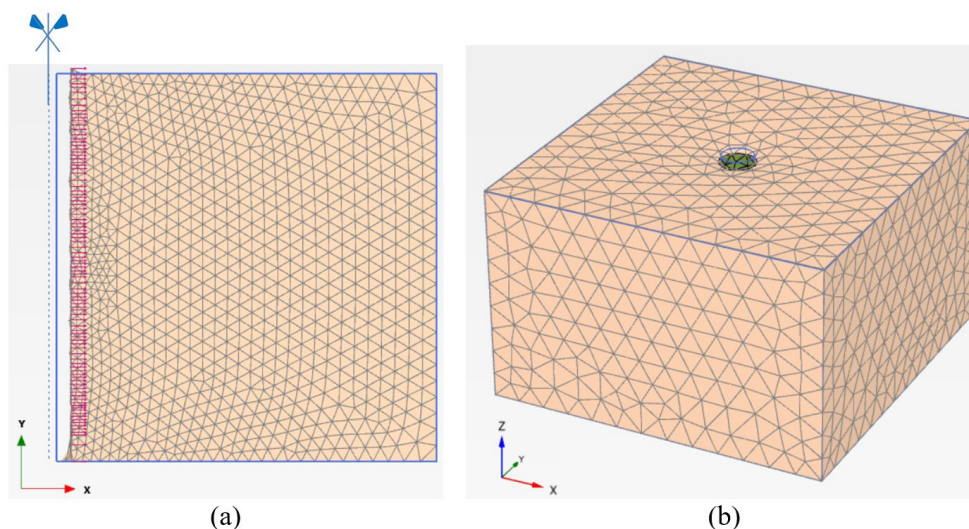
Figure 3. Numerical simulations: (a) axisymmetric model; (b) three-dimensional model.

Table 1. Material parameters used in FEM simulations.

Material Properties	Soft clay	Sand column	Gravel column	RCDW column
	Soft Soil (SS)	Mohr-Coulomb (MC)	Mohr-Coulomb (MC)	Mohr-Coulomb (MC)
Saturated unit weight, $\gamma_{sat}\left(kN/m^3\right)$	17	20	20	19
Effective Young's modulus, $E'\left(kPa\right)$	-	80000	80000	35000
Effective friction angle, $\phi'(^o)$	25	40.5	43	42
Dilatancy angle, $\Psi(^o)$	0	10	12	10
Effective cohesion, $c'\left(kPa\right)$	3	0.1	0.1	0.1
Effective Poisson's ratio, ν'	0.15	0.3	0.3	0.3
Modified compression index, λ*	0.2	-	-	-
Modified swelling index, κ*	0.12	-	-	-
Lateral earth pressure coefficient, K_0	0.57	0.35	0.32	0.33
Hydraulic conductivity in x direction, K_x (m/day)	1.39×10^{-3}	7	7	7
Hydraulic conductivity in y direction, K_y (m/day)	1.39×10^{-3}	7	7	7
Hydraulic conductivity in z direction, K_z (m/day)	1.39×10^{-3}	7	7	7
Interface coefficient (R_{int})	0.4	0.9	0.9	0.9

Table 2. Geotextile encasement parameters used in FEM simulation.

Properties	Seam (circumferential direction)		No seam (vertical direction)
	Maximum tensile strength of seam (kN/m)	Tensile stiffness at 5% strain (kN/m)	Tensile stiffness (kN/m)
G1	30	120	950
G2	16	107	366
G3	8	53.4	160

The encased RCDW numerical prediction (Figure 4d) was the least accurate regarding the results obtained in the tests. The predicted variation of settlement with load is quite linear, whereas the experimental variation is a curve, resulting in a difference of 26% at the final loading stage for G3. The RCDW grains were broken bricks, concrete, and gravel that may significantly influence the column mechanical properties.
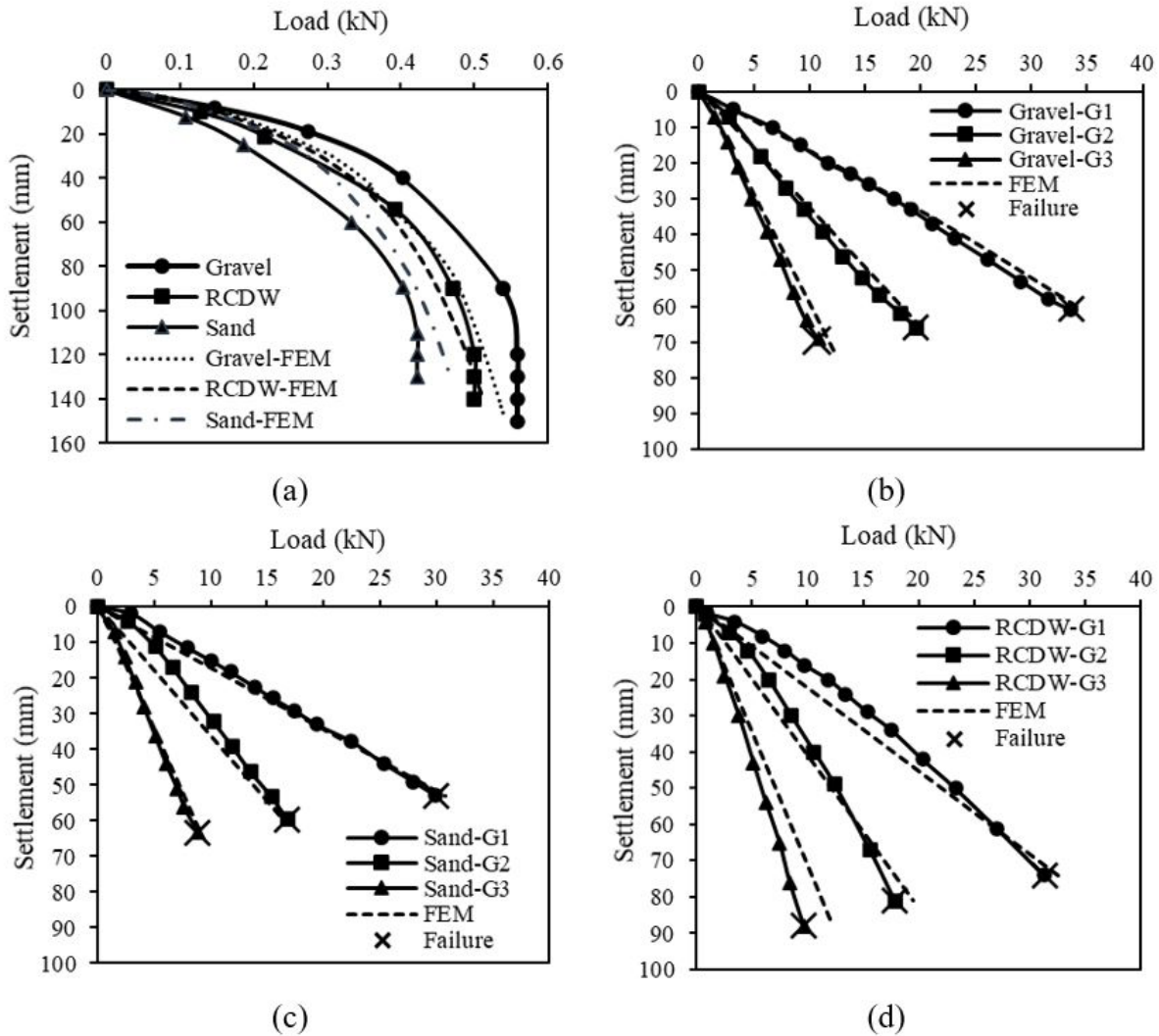
3.2 Excess pore water pressure

The piezometers installed show the excess pore water pressure produced during the column installation. The column loading tests started after the excess pore pressure was dissipated, which took approximately 45 hours. The numerical results compare rather well with those from the tests (Figure 5). The excess pore pressures reached a pick value during column installation and dropped down as time went by for all piezometers. However, the predicted reductions of pore pressures are steeper, showing a difference of approximately 200% at 18 hours of dissipation for P1. When it comes to the time needed for the full dissipation, the difference between predicted and measured results is between

1.5 to 2 hours. P3 and P4 show better comparisons between predicted and observed results than P1 and P2. During the loading stages, small values of excess pore water pressure were obtained by the piezometers. Piezometer P1, located at the bottom, close to the column, showed higher values of excess pore water pressure, as shown in Figure 6.
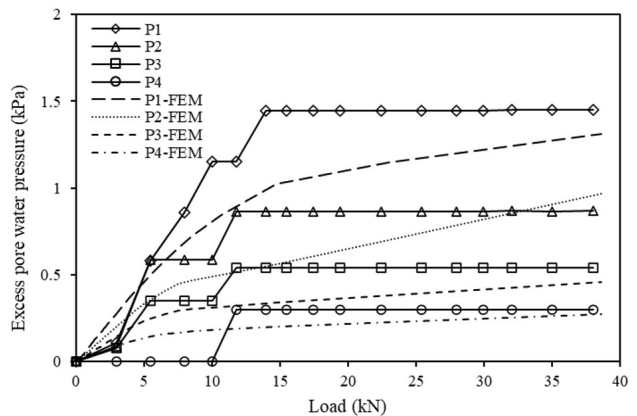
3.3 Soft soil undrained shear strength

Predicted and observed results in Figure 7 show some improvements in the undrained shear strength of the surrounding soil after the column was installed and the excess pore pressure dissipated. The undrained shear strength (S_u) in laboratory tests and numerical analysis was obtained from the vane shear tests and principal stresses, respectively. The test results show that values of S_u at the depths of 20 cm, 40 cm, 60 cm, and 80 cm increased by approximately 200% at 30 mm from the column. No increase in undrained strength was observed at 70 mm from the column. Hence, the diameter of the region (d_s, smear zone) disturbed by the column installations was 1.8 to 1.9 times the column diameter (d_c). However, the numerical analysis predicted values of ds greater than 1.9d_c as the soil
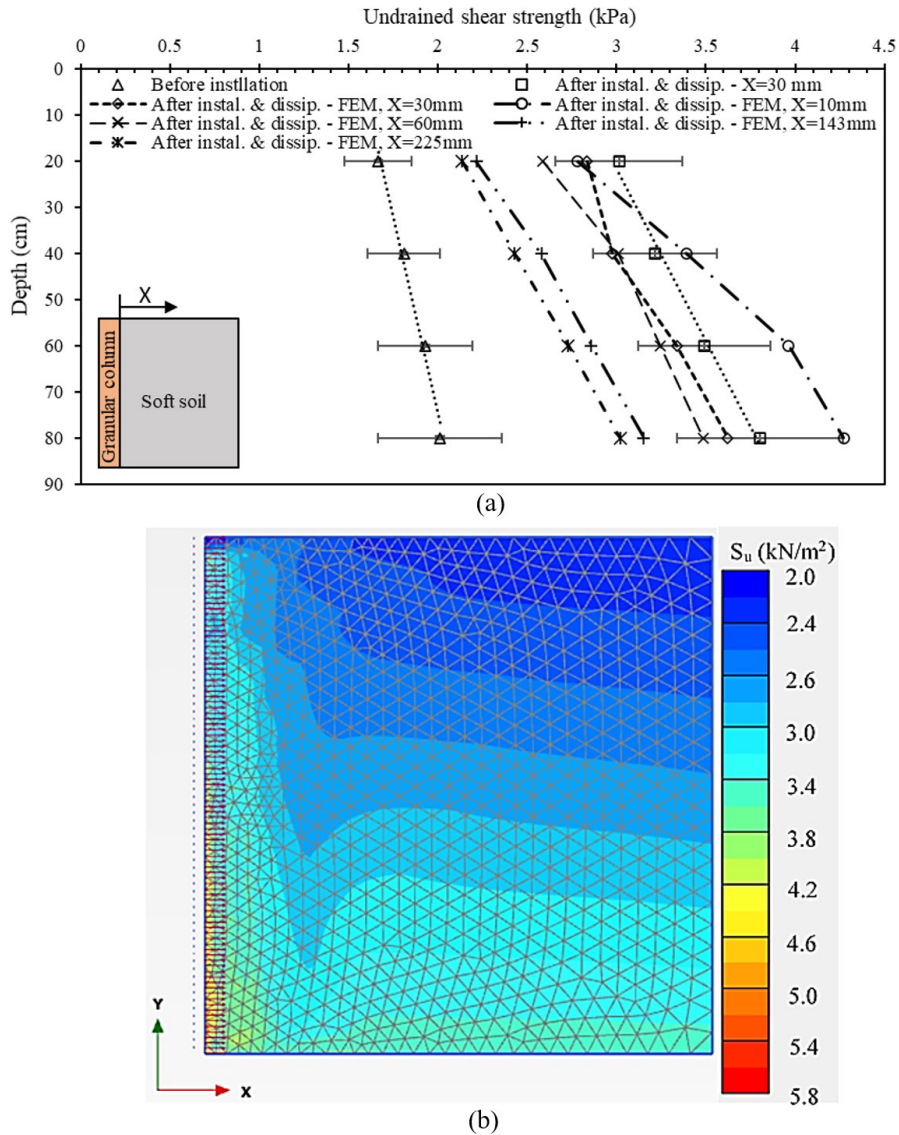
Figure 4. Load-settlement curves: (a) conventional columns; (b) encased gravel column; (c) encased sand column; (d) encased RCDW column.
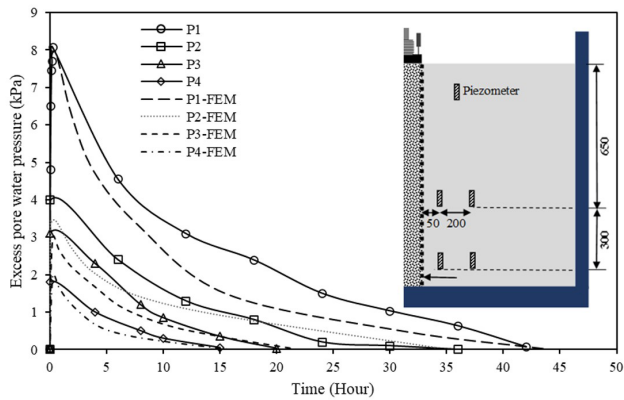
Figure 5. Excess pore water pressure during the column installation (dimensions in mm).

Figure 6. Excess pore water pressure during loading.

Figure 7. Changes of undrained shear strength with depth: (a) comparison between numerical and measured results and (b) numerical results.

undrained shear strength increases when it consolidates. The numerical results at 30 mm from the column depict reasonable agreements with those from the tests. These results show that at 10 mm, the values of S_u were approximately 3 times greater than the initial values (before column installation) at the depths of 60 cm and 80 cm.
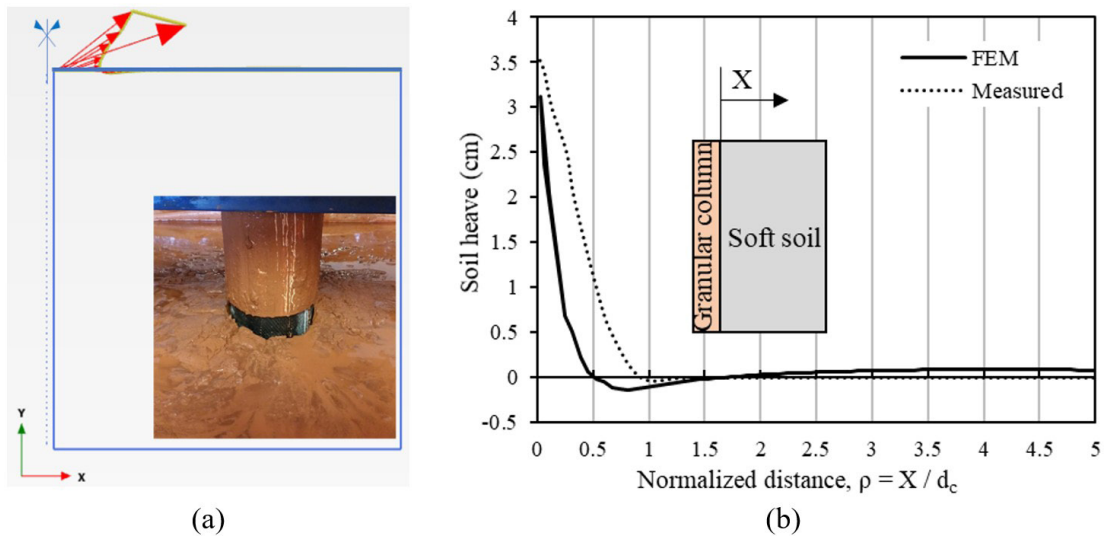
3.4 Soil heave

The predicted and measured results show that the column installation displaces the soil circumferentially (Figure 8), leading to soil surface heave. These results show that the soil experienced a heave displacement approximately equal to half the column radius along the column perimeter. However, regarding the diameter of the region around the column that

underwent heave (d_h), a significant difference can be noted between predicted and observed results so that the former is half the latter one.

3.5 Failure and deformation mechanisms

The loading tests were carried out to obtain the column's maximum loading capacity. As shown in Figures 9a and 9b, the column failed at a depth of 0.15 to 0.18 m (from the column top). The load on the column top caused it to bulge, leading to geotextile encasement failure. The numerical analyses indicated that the column experienced excessive bulging at the same depths, as shown in Figure 9c. Figure 10 shows that the tensile forces developed in the geotextile encasement slightly exceeded or were close to the encasement maximum tensile strength

Figure 8. Soil heave after column installation: (a) soil surface; (b) predicted and measured results.
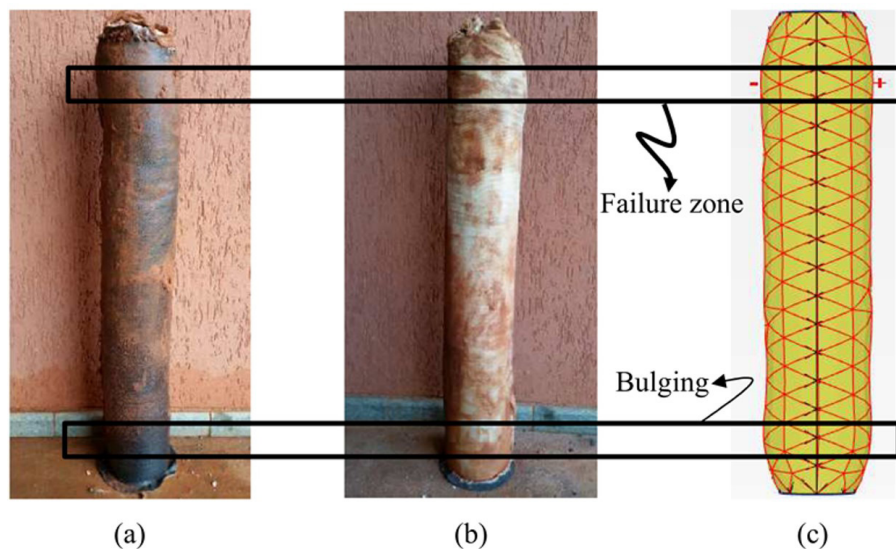
Figure 9. Columns after loading: (a) and (b) exhumed columns after testing; (c) column shape obtained from numerical analyses.

(marked with red circles in Figure 10) between elevations 0.07 m and 0.15 m and between elevations 0.8 m and 0.94 m.

3.6 Breakage of the granular column particles

The gravel and RCDW columns were divided into five sections to evaluate the breakage (B_g) of particles of the column infill material using Marsal's (1967) procedure, as shown in Figure 11. The results (Table 3) show that the gravel and RCDW columns (encased with G1) underwent particle breakage of as much as 15.89% and 20.94%, within sections 1 and 2 ($2d_c$), respectively. The numerical results predicted that within these sections the column experienced significant shear strains (Figure 12) and confinement (from the encasement, Figure 13), which can be the reason for the column infill breakage. Sieving tests on the infill material did not show any significant level of particle breakage in sections 3, 4, and 5.

At the end of every test, the region around the column top experienced an active state of stresses resulting in tension cracks development up to a radius (R_{TC}) of 22.5 cm (Figure 14a). It can also be verified by checking the tension cut-off points in the numerical analyses that show the region in which the soil fails in tension. The predicted results (Figure 14b) show that R_{TC} extended up to a radius of 22.7 cm, which compares well with the test results.
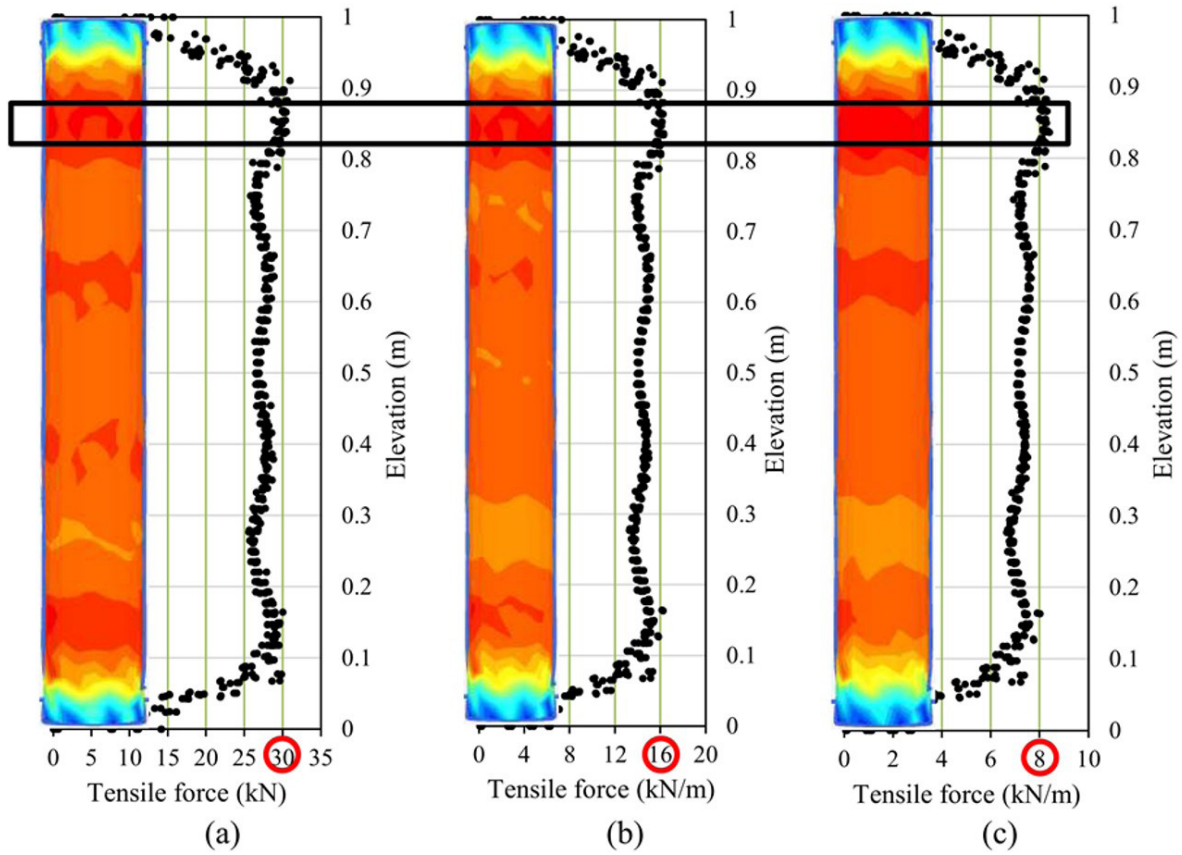
Figure 10. The tensile force along the column height (a) G1; (b) G2; (c) G3.
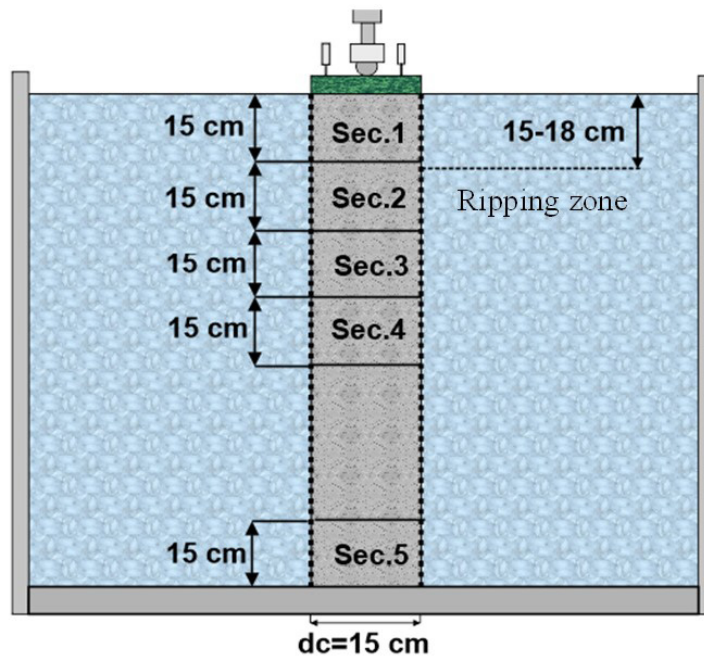

**Figure 11.** Column sections used to measure particle breakage.

Table 3. Particle breakage index for the encased gravel and CW column.

Geotextile	Column type	Section	Particle breakage index – B_g (%)	Average of B_g (%)
G-1	Gravel column	Sec.1	14.11	15.89
		Sec.2	17.67	
	RCDW column	Sec.1	17.18	20.94
		Sec.2	24.7	
G-2	Gravel column	Sec.1	6.82	7.04
		Sec.2	7.27	
	RCDW column	Sec.1	8.11	9.34
		Sec.2	10.58	
G-3	Gravel column	Sec.1	1.34	1.55
		Sec.2	1.77	
	RCDW column	Sec.1	2.65	3.3
		Sec.2	3.95	
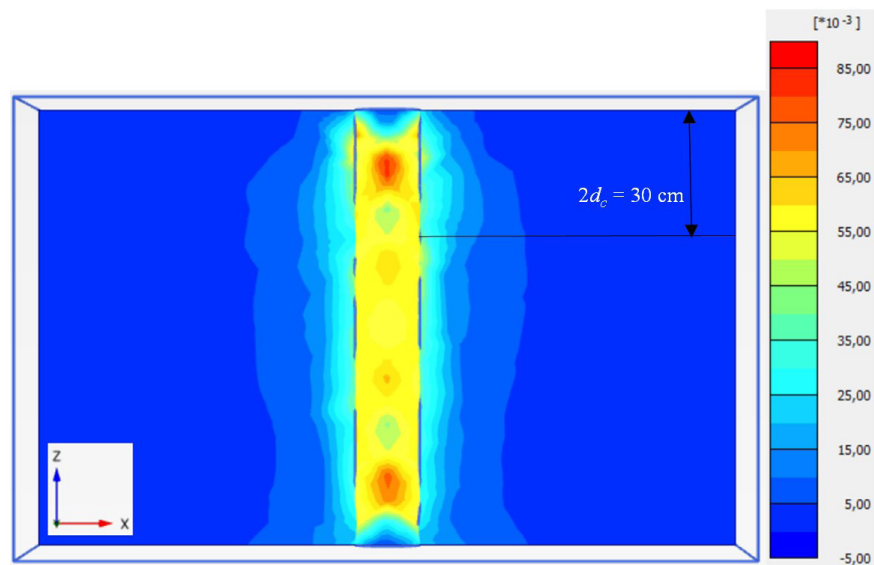
Figure 12. Shear strains along the column.
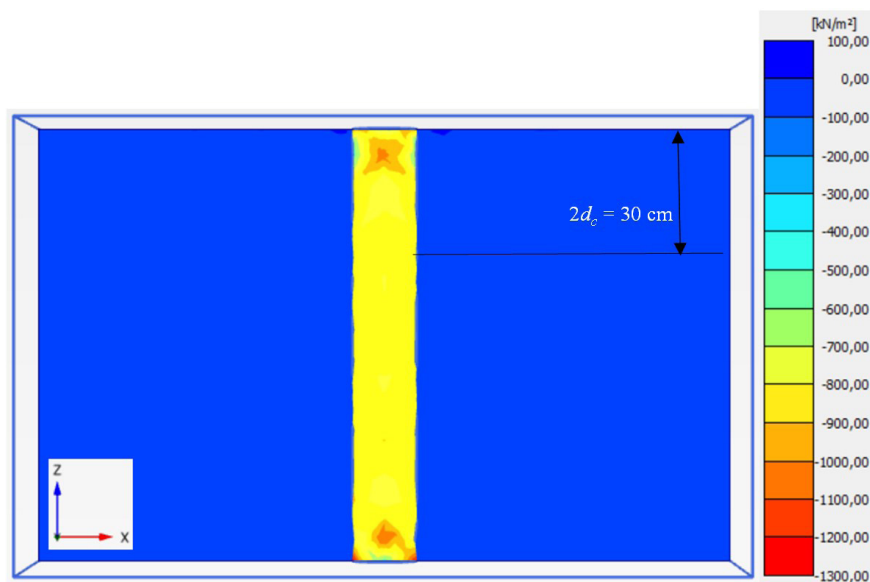
Figure 13. Total mean stress along the column.

(a)   (b)
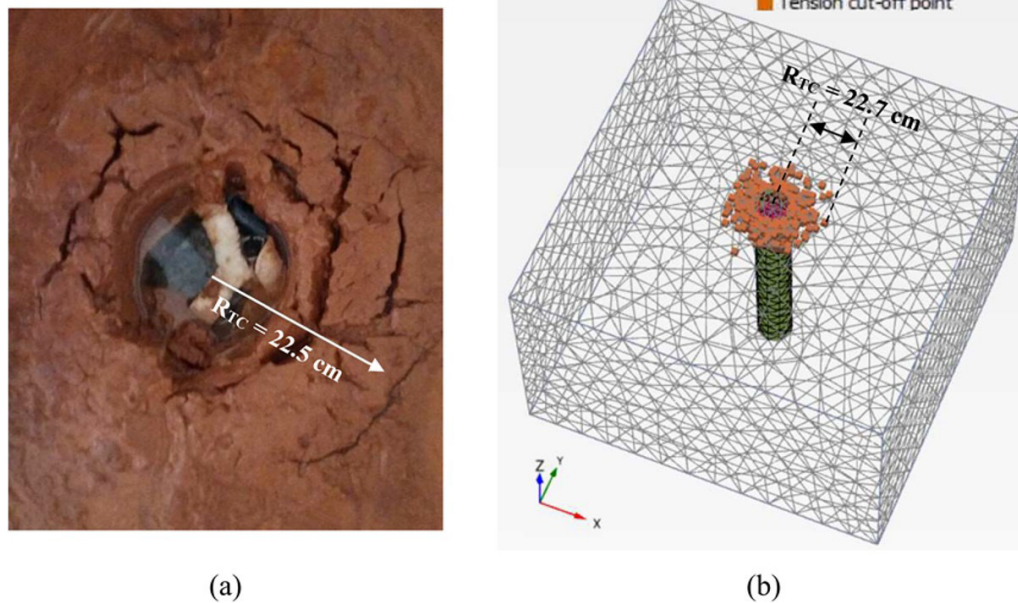
Figure 14. Tension cracks at the soil surface: (a) test result; (b) numerical result.

4. Conclusions

This study compared finite element predictions with results from large scale laboratory tests for a better understanding on the behavior of geosynthetic encased columns in soft soils. The main conclusions of the study are summarized below:

- The column infill type (sand, gravel, and RCDW) did not contribute significantly to the bearing capacity of the conventional (uncased) column. On the other hand, the bearing capacity of the encased column was influenced by the type of infill material, with greater value for the gravel column;

- The predicted load-settlement results for the conventional and encased sand and gravel columns compared satisfactorily with the experimental results, except for the case of RCDW infill, which can be a consequence of higher particle breakage of RCDW;

- The results obtained by the numerical analyses and laboratory tests showed the contribution of the granular column in the dissipation of the excess pore water pressures;

- The experimental results showed that the undrained strength of the soft soil (S_u) was increased up to a radial distance of 1.9 times the column diameter (d_c), after pore pressure dissipation. On the other hand, the numerical results predicted S_u increases even beyond $1.9d_c$;

- The soil heave displacement predicted by the numerical analyses compared well with that measured in the laboratory tests. Nevertheless, the radius of the region that underwent heave in the tests was twice that predicted by the numerical analysis;

- The numerical results accurately predicted the depths where the geotextile encasement failed. Furthermore, the results showed that the encasement experienced the highest tensile forces within regions with lengths equal to two times the column diameter at the column top and bottom.

Acknowledgments

Declaration of interest

The authors have no conflicts of interest to declare. All co-authors have observed and affirmed the contents of the paper and there is no financial interest to report.

Authors' contributions

Nima Rostami Alkhorshid: conceptualization, Methodology, Data curation, Software, Writing – original draft. Gregório Luís Silva Araújo: funding acquisition, Supervision, Validation, Writing – review & editing. Ennio Marques Palmeira: supervision, Validation, Writing – review & editing.

List of symbols

γ_{sat}	Saturated unit weight
E'	Effective Young's modulus
ϕ'	Effective friction angle
Ψ	Dilatancy angle
c'	Effective cohesion
v'	Effective Poisson's ratio
λ^*	Modified compression index
κ^*	Modified swelling index
K_0	Lateral earth pressure coefficient
K_x	Hydraulic conductivity in x direction
K_y	Hydraulic conductivity in y direction
K_z	Hydraulic conductivity in z direction
R_{int}	Interface coefficient

References

Alexiew, D., & Raithel, M. (2015). Geotextile-encased columns: case studies over twenty years. In B. Indraratna, J. Chu & C. Rujikiatkamjorn (Eds.), *Ground improvement case histories* (pp. 451-477). Kidlington: Elsevier. https://doi.org/10.1016/B978-0-08-100192-9.00017-X.

Ali, K., Shahu, J.T., & Sharma, K.G. (2012). Model tests on geosynthetic-reinforced stone columns: a comparative study. *Geosynthetics International*, 19(4), 292-305. http://dx.doi.org/10.1680/gein.12.00016.

Alkhorshid, N.R. (2012). *Numerical analysis of soft clay reinforced with stone columns* [MSc thesis, Eastern Mediterranean University]. Eastern Mediterranean University's repository. Retrieved in July 9, 2021, from http://hdl.handle.net/11129/1259

Alkhorshid, N.R. (2017). *Analysis of geosynthetic encased columns in very soft soil* [PhD thesis, University of Brasília]. University of Brasília's repository. Retrieved in July 9, 2021, from https://repositorio.unb.br/handle/10482/32033.

Alkhorshid, N.R., Araujo, G.L., & Palmeira, E.M. (2018). Behavior of geosynthetic-encased stone columns in soft clay: numerical and analytical evaluations. *Soils and Rocks*, 41(3), 333-343. http://dx.doi.org/10.28927/SR.413333.

Alkhorshid, N.R., Araujo, G.L., & Palmeira, E.M. (2019). Large-scale load capacity tests on a geosynthetic encased column. *Geotextiles and Geomembranes*, 47(5), 632-641. http://dx.doi.org/10.1016/j.geotexmem.2019.103458.

Alkhorshid, N.R., Araujo, G.L., & Palmeira, E.M. (2020). Large scale tests on geotextile encased stone columns. In *Proc. 4th Pan American Conference on Geosynthetics* (pp. 1-7). Rio de Janeiro: IGS.

Alkhorshid, N.R., Araujo, G.L., & Palmeira, E.M. (2021). Consolidation of soft clay foundation improved by geosynthetic-reinforced granular columns: numerical evaluation. *Journal of Rock Mechanics and Geotechnical Engineering*, 13(5), 1173-1181. http://dx.doi.org/10.1016/j.jrmge.2021.03.004.

Alkhorshid, N.R., Nalbantoglu, Z., & Araujo, G.L. (2014). 3D analysis of full scale stone column reinforced soft clay: numerical evaluation. In *Proc. XVII Congresso Brasileiro de Mecânica dos Solos* (pp. 1-6). Goiânia: ABMS.

Almeida, M.S., Hosseinpour, I., & Riccio, M. (2013). Performance of a geosynthetic-encased column (GEC) in soft ground: numerical and analytical studies. *Geosynthetics International*, 20(4), 252-262. http://dx.doi.org/10.1680/gein.13.00015.

Araujo, G.L., Palmeira, E.M., & Cunha, R.P. (2009). Behaviour of geosynthetic-encased granular columns in porous collapsible soil. *Geosynthetics International*, 16(6), 433-451. http://dx.doi.org/10.1680/gein.2009.16.6.433.

Castro, J., & Karstunen, M. (2010). Numerical simulations of stone column installation. *Canadian Geotechnical Journal*, 47(10), 1127-1138. http://dx.doi.org/10.1139/T10-019.

Castro, J., & Sagaseta, C. (2011). Deformation and consolidation around encased stone columns. *Geotextiles and Geomembranes*, 29(3), 268-276. http://dx.doi.org/10.1016/j.geotexmem.2010.12.001.

Castro, J., & Sagaseta, C. (2013). Influence of elastic strains during plastic deformation of encased stone columns. *Geotextiles and Geomembranes*, 37, 45-53. http://dx.doi.org/10.1016/j.geotexmem.2013.01.005.

Cengiz, C., & Guler, E. (2020). Load bearing and settlement characteristics of Geosynthetic Encased Columns under seismic loads. *Soil Dynamics and Earthquake Engineering*, 136, 106244. http://dx.doi.org/10.1016/j.soildyn.2020.106244.

Chen, J.F., Li, L.Y., Zhang, Z., Zhang, X., Xu, C., Rajesh, S., & Feng, S.Z. (2020). Centrifuge modeling of geosynthetic-encased stone column-supported embankment over soft clay. *Geotextiles and Geomembranes*, 49(1), 210-221. http://dx.doi.org/10.1016/j.geotexmem.2020.10.021.

De Mello, L.G., Mondolfo, M., Montez, F., Tsukahara, C.N., & Bilfinger, W. (2008). First use of geosynthetic encased sand columns in South America. In *Proc. 1st Pan-American Geosynthetics Conference* (pp. 1332-1341), Cancun, Mexico.

Gniel, J., & Bouazza, A. (2009). Improvement of soft soils using geogrid encased stone columns. *Geotextiles and Geomembranes*, 27(3), 167-175. http://dx.doi.org/10.1016/j.geotexmem.2008.11.001.

Keykhosropur, L., Soroush, A., & Imam, R. (2012). 3D numerical analyses of geosynthetic encased stone columns. *Geotextiles and Geomembranes*, 35, 61-68. http://dx.doi.org/10.1016/j.geotexmem.2012.07.005.

Khabbazian, M., Kaliakin, V.N., & Meehan, C.L. (2010). Numerical study of the effect of geosynthetic encasement on the behaviour of granular columns. *Geosynthetics International*, 17(3), 132-143. http://dx.doi.org/10.1680/gein.2010.17.3.132.

Li, L.Y., Rajesh, S., & Chen, J.F. (2020). Centrifuge model tests on the deformation behavior of geosynthetic-encased

stone column supported embankment under undrained condition. *Geotextiles and Geomembranes*, http://dx.doi.org/10.1016/j.geotexmem.2020.11.003.

Marsal, R.J. (1967). Large scale testing of rockfill materials. *Journal of the Soil Mechanics and Foundations Division*, 93(2), 27-43. http://dx.doi.org/10.1061/JSFEAQ.0000958.

Mohapatra, S.R., Rajagopal, R., & Sharma, J. (2017). 3-Dimensional numerical modeling of geosynthetic-encased granular columns. *Geotextiles and Geomembranes*, 45(3), 131-141. http://dx.doi.org/10.1016/j.geotexmem.2017.01.004.

Nagula, S.S., Nguyen, D.M., & Grabe, J. (2018). Numerical modelling and validation of geosynthetic encased columns in soft soils with installation effect. *Geotextiles and Geomembranes*, 46(6), 790-800. http://dx.doi.org/10.1016/j.geotexmem.2018.07.011.

Pulko, B., & Logar, J. (2017). Fully coupled solution for the consolidation of poroelastic soil around geosynthetic encased

stone columns. *Geotextiles and Geomembranes*, 45(6), 616-626. http://dx.doi.org/10.1016/j.geotexmem.2017.08.003.

Xue, J., Liu, Z., & Chen, J. (2019). Triaxial compressive behaviour of geotextile encased stone columns. *Computers and Geotechnics*, 108, 53-60. http://dx.doi.org/10.1016/j.compgeo.2018.12.010.

Yoo, C., & Lee, D. (2012). Performance of geogrid-encased stone columns in soft ground: full-scale load tests. *Geosynthetics International*, 19(6), 480-490. http://dx.doi.org/10.1680/gein.12.00033.

Zhang, L., Xu, Z., & Zhou, S. (2020). Vertical cyclic loading response of geosynthetic-encased stone column in soft clay. *Geotextiles and Geomembranes*, 48(6), 897-911. http://dx.doi.org/10.1016/j.geotexmem.2020.07.006.

Zhang, Y., Chan, D., & Wang, Y. (2012). Consolidation of composite foundation improved by geosynthetic-encased stone columns. *Geotextiles and Geomembranes*, 32, 10-17. http://dx.doi.org/10.1016/j.geotexmem.2011.10.006.